J. Plasma Phys. (2021), *vol*. 87, 845870201
Published by Cambridge University Press
doi:10.1017/S0022377821000131

Long-pulse plasma source for SMOLA helical mirror

Ivan A. Ivanov[1],†, **V. O. Ustyuzhanin**[1,2], **A. V. Sudnikov**[1] and **A. Inzhevatkina**[1]

[1]Budker Institute of Nuclear Physics, 11 Lavrentyev av., Novosibirsk 630090, Russia

[2]Novosibirsk State University, 1 Pirogov st., Novosibirsk 630090, Russia

(Received 6 July 2020; revised 26 January 2021; accepted 1 February 2021)

A plasma gun for forming a plasma stream in the open magnetic mirror trap with additional helicoidal field SMOLA is described. The plasma gun is an axisymmetric system with a planar circular hot cathode based on lanthanum hexaboride and a hollow copper anode. The two planar coils are located around the plasma source and create a magnetic field of up to 200 mT. The magnetic field forms the magnetron configuration of the discharge and provides a radial electric insulation. The source typically operates with a discharge current of up to 350 A in hydrogen. Plasma parameters in the SMOLA device are $T_i \sim 5$ eV, $T_e \sim 5$–40 eV and $n_i \sim (0.1\text{–}1) \times 10^{19}$ m^{-3}. Helium plasma can also be created. The plasma properties depend on the whole group of initial technical parameters: the cathode temperature, the feeding gas flow, the anode-cathode supply voltage and the magnitude of the cathode magnetic insulation.

Key words: plasma devices, plasma properties, electric discharges

1. Introduction

Open magnetic systems, which are significantly different from each other in their design and operating principles, theoretically allow working with non-tritium and neutron-free reactions, which makes it possible for such plants to function for longer without expensive reconstructions (Anikeev *et al*. 2015; Gota *et al*. 2019). The following parameters were obtained in experiments on plasma confinement in open magnetic traps: high relative pressure ($\beta \approx 60\,\%$, Simonen *et al*. 2010), average hot ion temperature of 12 keV and electron temperature of up to 0.9 keV in a stable mode (Bagryansky *et al*. 2015).

However, the key problem remains unresolved: the suppression of the longitudinal losses of particles and energy, which is the reason for the short plasma confinement time. The existing method of multiple mirror suppression of axial heat flux in combination with a gas-dynamic central cell (Postupaev *et al*. 2017) can provide an effective mirror ratio of about 100. One of the new options for multiple-mirror plasma confinement is the concept of helicoidal field confinement (Beklemishev 2013).

This concept is based on the creation of magnetic mirrors moving in the plasma reference frame using a spiral magnetic field. In this case, the plasma rotates in

† Email address for correspondence: i.a.ivanov@inp.nsk.su

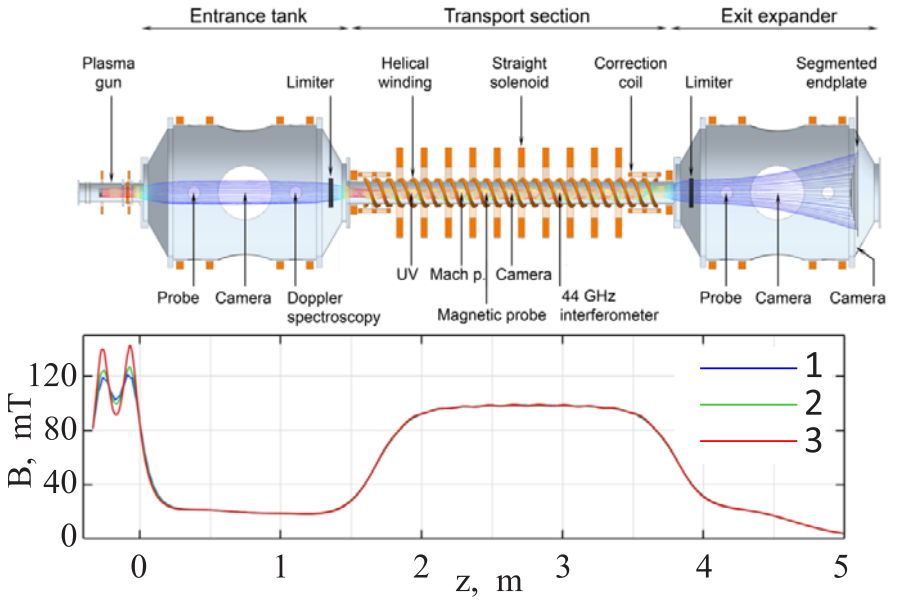

FIGURE 1. SMOLA helical mirror. Origin $z = 0$ corresponds to the plasma gun exit; 1, magnetic field induction on the axis; 2, $r = 3$ cm; 3, $r = 6$ cm.

$E \times B$ fields. Thus, depending on the direction of the magnetic disturbances motion relative to the plasma flow, the force acting on the particles leads either to the deceleration of the plasma and its transfer back to the central cell of the trap, or to the acceleration of the plasma jet (Beklemishev 2015). Theoretical calculations (Beklemishev 2016) predict that the plasma confinement time will exponentially depend on the length of the magnetic system, which is much more efficient than in other open magnetic systems: linear dependence (mirror cell), quadratic (multi-mirror trap).

To verify the concept of helical confinement, the SMOLA device was created in the Budker Institute of Nuclear Physics of the Russian Academy of Science (BINP SB RAS) in 2017 (Postupaev *et al*. 2016; Sudnikov *et al*. 2017). The presence of the axial plasma flow suppression was already demonstrated in the first experiments (Sudnikov *et al*. 2019) with an incomplete configuration of subsystems of the device.

The SMOLA device consists of an input expander with discharge-forming system (plasma source), figure 1, transport section with helical and straight solenoids for decelerating or accelerating the plasma flow depending on the direction of plasma rotation and exit expander with radial segmented endplate. The confining magnetic field in the transport section $B_{\max} = 0.1$–0.3 T with the tuneable average mirror ratio along the magnetic field line $R_{\text{mean}} = 1$–2. The radial electric field reaches of up to $E_r \sim 1$ kV m^{-1} and is created by longitudinal plasma conductivity from the cathode biasing of the plasma source.

The present work is devoted to the study of the creation process of plasma in the SMOLA device. The plasma discharge system is the axisymmetric system using the magnetically insulated discharge with magnetron configuration. The plasma source is based on a similar discharge configuration as described by Akhmetov *et al*. (2016) and was used for explanation of the plasma formation in PSI-2 (Kreter *et al*. 2017). In fact, almost all high-current plasma guns use magnetic isolation to efficiently generate the plasma stream. For example, in the work of Binderbauer *et al*. (2015), the plasma gun

https://doi.org/10.1017/S0022377821000131 Published online by Cambridge University Press

has a hollow cathode and effectively generates the plasma stream with a plasma density of approximately 10^{19} m^{-3} during about 5 ms. In our system, the cathode is thermionic hot LaB_6 (see, for example, Lafferty 1951) and has planar circular geometry. Such a cathode configuration is often used for wide plasma stream creation at densities up to 10^{19} m^{-3} in long magnetically insulated linear systems (see, for example, Gekelman *et al*. 2016). Using an infrared heater (such as the tungsten spiral described in Goebel, Hirooka & Sketchley 1985), the cathode is heated up to $T \sim 1900$ K. The electrons emitted by the cathode ionize the working gas and, thus, the plasma flow is generated with a density of $n \sim 10^{-19}$ m^{-3} and $T \sim 5$ eV near the gun. The axial magnetron discharge configuration is characterized by a finite radial gap between the field line starting from the edge of the cathode and the inner anode surface. To optimize the transport and confinement of the plasma in the trap, it is important to monitor and regulate the primary parameters of the plasma jet. For this purpose, a diagnostic complex has been created. It includes radial movable Langmuir probes and measuring instruments for electrical parameters of discharge, vacuum parameters, as well as power systems control for all high-power circuits.

The key task of this paper is the description of the plasma formation process in the device. First, the influence of setting of floating diaphragms inside the plasma gun has been determined. The other parameters, such as the gas puffing, the voltage at the cathode and its temperature also affect the parameters of the resulting plasma, but in this paper, the plasma parameters are given for comparison in two configurations of the gun (with and without the diaphragms). Optimization of the gun operating modes was primarily done for the generation of sufficient discharge current, which affects the plasma density, as well as the efficiency of gas utilization and the amount of residual gas in the trap in the presence of plasma.

2. Plasma gun layout

The plasma source is an axisymmetric system with planar circular hot cathode based on LaB_6, hollow copper anode, two main magnetic coils and a vacuum chamber 14 cm in diameter and 48 cm in length. LaB_6 as a cathode material has some advantages: it can be exposed to air and water leaks and still be reused. It does not have to be recoated when the machine is open to air. The material can withstand the higher ion fluxes associated with higher current discharges. Although LaB_6 must be heated to nearly twice as hot as BaO, it has a higher electron emission per unit area and therefore can produce higher plasma densities and temperatures than oxide-coated cathodes. The cathode is a circular disc of sintered LaB_6 powder with diameter $D = 5$ cm and thickness $h = 3$ mm. It is indirectly heated by the radiation of a tungsten spiral, which is located behind the cathode. This spiral heats the cathode up to $T \approx 1900$ K. The heater current is supplied through an electrically insulated feeder at the centre of the cathode flange and closes on the vacuum side of this flange. The cathode assembly has molybdenum foil thermal shields to reduce losses and minimize heating power. Thus, 800 W power is required to heat the cathode up to the operating temperature.

Figure 2 shows a layout of the plasma source with sketchy feeding diagram. Electrons are emitted from the LaB_6 cathode surface and accelerated through the anode towards the right-hand side of the figure. Anode–cathode isolation is created by a longitudinal magnetic field so the magnetic field line starting on the edge of the cathode usually lies about 5 mm away from the anode. Structurally, the cathode is isolated from the anode by two insulators with a long metal cylindrical insert in the middle, called the gun shell. This insert is designed to perform several functions. The first is to protect the insulators from ultraviolet radiation and fast neutral particles, thus preventing the breakdown of insulators. The second is to create a volume with a floating potential around the cathode in which the

https://doi.org/10.1017/S0022377821000131 Published online by Cambridge University Press

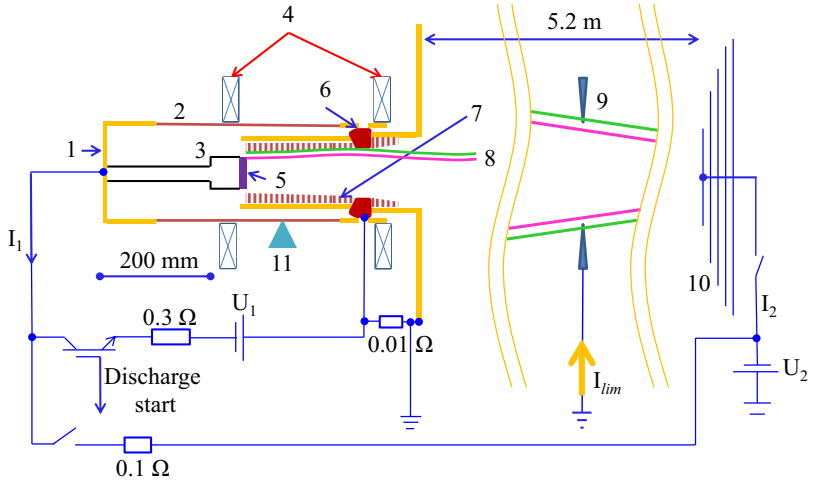

FIGURE 2. Plasma gun layout with the electrical circuit. The designations: 1, cathode-holding flange; 2, isolated gun shell; 3, cathode holder; 4, magnetic coils; 5, LaB_6 cathode; 6, anode; 7, floating molybdenum diaphragms; 8, magnetic field lines (red, the line touching the edge of the cathode; green, anode); 9, plasma limiter in entrance expander; 10, plasma dump plates; 11, gas puffing systems.

bulk of collisions of electrons with the gas filled into the gun volume will occur, thus carrying out ionization. The inner part of this insert is covered by molybdenum foil to reduce the formation of unipolar plasma arcs from the surface. The whole vacuum volume of the gun is about $RV_G \approx 4.4 \times 10^3 \mathrm{cm}^3$.

In the first, entrance, expander, before the transport section, the limiter is mounted. Its potential is usually grounded and the current flowing to it from the plasma is measured. Its inner diameter is projected to anode through magnetic lines.

After the transport section, the plasma stream passes to the exit magnetic expander with a mirror ratio of about $R \sim 100$. In the expander a radially segmented electrically insulated plasma dump is mounted. In the typical experimental regime, the anode of the plasma gun is projected by the magnetic field lines to the outermost electrode of the dumper. It consists of five concentric molybdenum electrodes with independently controlled potentials (potential difference between closest electrodes is up to 50 V). The external diameter of the plasma dump is $D \sim 0.65$ m. The central plate has a constant negative potential $U \sim -300$ V in a typical experimental shot. In addition, the plasma rotation in the discussed experiments is driven by the dump plates potentials and the gun cathode potential.

Electrical feeding of the plasma gun is carried out by a capacitor through the IGBT transistor and resistive ballast. The inductive impedance of feeders is negligible in relation to ballast. The feeding capacitor consists of series of the supercapacitors with a total capacity of 10 F. It charged up to $U = -150 - 300$ V.

The magnetic field is created by two coils placed coplanarly to the cathode and the anode correspondingly. They are fed independently, so it allows the required magnetic insulation and gun magnetic mirror ratio to be created with respect to the entrance expander of the device.

The gas feeding of the plasma gun is carried out by two independent gas valves. The first serves for the fast filling of the gun volume and is opening only for the first 3–10 ms with

https://doi.org/10.1017/S0022377821000131 Published online by Cambridge University Press

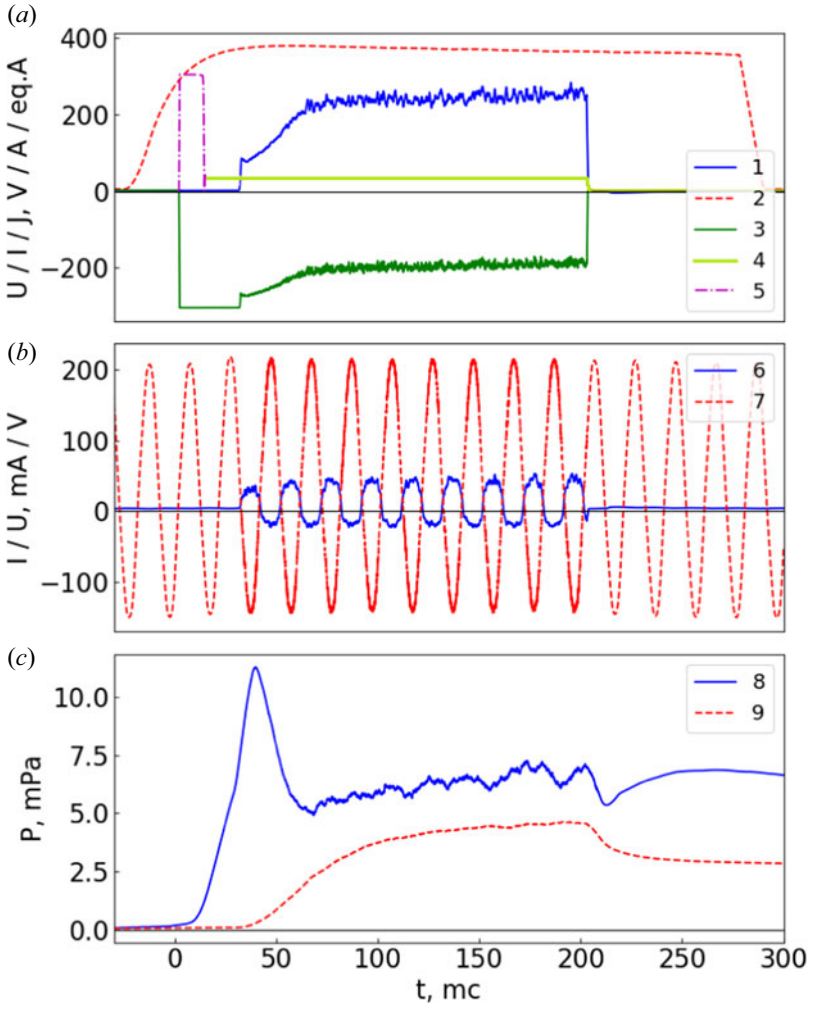

FIGURE 3. Typical experimental diagrams of gun subsystems and some diagnostics in optimized operating mode, shot #6408. Designations: 1, discharge current; 2, magnetic coil current; 3, cathode potential; 4, equivalent gas flow from the slow valve; 5, equivalent gas flow from the fast valve; 6, double Langmuir probe current; 7, double Langmuir probe potential; 8, entrance expander pressure; 9, exit expander pressure.

the discharge initiation and begins gas puffing simultaneously with the switching on of the cathode voltage. The amount of puffed hydrogen atoms is close to 10^{19}. The second works during whole plasma discharge and carries out the stationary gas feeding through the thin long capillary for dumping the pulsations and smoothing out of the gas flow. The H_2 gas puff rate is within about 10^{19}–10^{20} atoms s^{-1} (typical $J_{H_2} \approx 6.5 \times 10^{-19}$atoms $s^{-1} \approx$ 20 eq.A) and is regulated by the working gas pressure on the high-pressure side of the valve. It lies within the limits of $10^{-1} - 2$ bar.

The typical diagrams of the plasma subsystems in optimized operating mode are shown in figure 3(*a*). First, the cathode heating switches off because the Lorentz force of the current in the tungsten spiral in the external magnetic field of the gun can break the heater.

https://doi.org/10.1017/S0022377821000131 Published online by Cambridge University Press

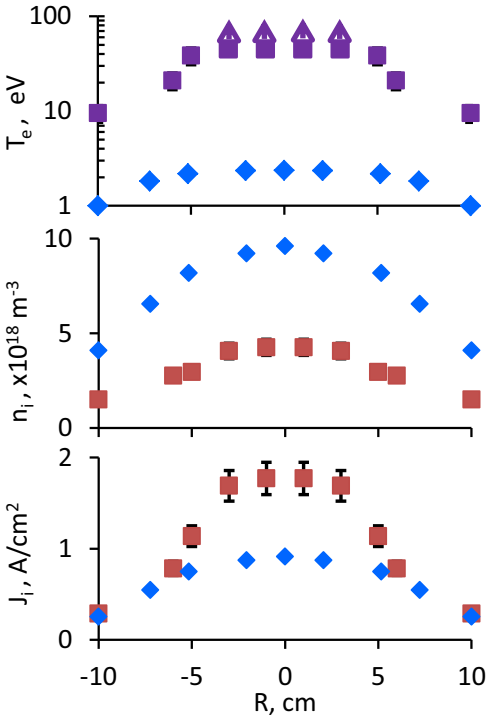

FIGURE 4. The radial profiles of electron temperature, ion plasma density and ion flux calculated from *I–V* characteristic of double Langmuir probe. Designations: squares, plasma parameters after the floating diaphragms were installed inside the plasma gun (figure 2, num. 7); diamonds, before installation of the diaphragms. The arrows mean that the *I–V* probe characteristic gives a higher electron temperature than the indicated points.

Then, the confining magnetic field is switched on. It is created by different axial coils powered by the supercapacitors with corresponding voltages.

When the current in the coils reaches the stationary phase, the fast gas valve opens, and the cathode potential is switched on. This time corresponds to $t = 0$ ms on the graphs. When the gas concentration in the entrance expander reaches $n_{H_2} \sim (2-3) \times 10^{18}\mathrm{m}^{-3}$ the self-confining discharge ignites. This is seen in the cathode current diagram (figure 3*a*). The temporal delay is about 30 ms and is determined by the gas puffing rate. These data can be obtained from gas pressure measurements, see figure 3(*c*). From these measurements one can estimate the gas concentration inside the plasma gun volume by the value $n_{\mathrm{H}_2} \sim 10^{21}\ \mathrm{m}^{-3}$.

The temporal stationarity in the discharge begins about 30 ms after the cathode current starts. During these first 30 ms, the plasma gun current approximately doubles, and at the same time the pressure in the entrance expander tank stabilizes at around 3–6 mPa (note that all ionization vacuum gauges have doubtful accuracy owing to the plasma ultraviolet emission: we covered them up from direct radiation to minimize this effect, but accurate gas pressure estimation can only be done just after plasma disappearance). All diagnostics show that the plasma macroscopic parameters stay almost constant from this moment as well. The plasma termination is determined by switching off of the cathode voltage. However, the gun feeding system can produce up to 1.6 s discharge.

https://doi.org/10.1017/S0022377821000131 Published online by Cambridge University Press

The local plasma parameters are determined by the double Langmuir probes placed on radial movable motorized sticks. The probes are installed along the SMOLA system at distances $z = 0.4$, 2.5 and 4 m from the exit of the plasma gun. Data from the probe at $z = 0.4$ m are presented in figure 3(*b*). It shows the plasma density of $n_i \approx 0.8 \times 10^{19}$ m^{-3} and electron temperature $T_e \sim 40$ eV at the centre of the system during the regular temporal period, at $t > 70$ ms in the diagram. The ion density profile at this axial point during a regular discharge period is shown in figure 4. The radius of half density, $r_0 \approx 9$ cm, is close to the anode value with respect to the magnetic flux conservation. The two different series of experimental data are shown in the figure. The best data correspond to the highest electron temperature and were obtained after installing the floating diaphragms inside the cathode–anode gap of the gun, see figure 2.

3. Discussion of the plasma discharge features

To provide cathode current, either thermal emission without current saturation is needed and then the Child's law is fulfilled or, in the other case, the Richardson–Laue–Dushman law is fulfilled with the saturation of the electron emission current. In our case the cathode current density (see figure 3, curve 1) of $J_C \approx 250$ A/$S_C \approx 13$ A cm^{-2} in the experiment can correspond to either of the cases, because the thermionic cathode-limiting current can reach more than 20 A cm^{-2}. Moreover, if we permit that the electron current is limited by the Richardson–Laue–Dushman law, then for LaB_6 (Goebel *et al*. 1985):

$$j_R \approx A \cdot T^2 \cdot exp\left(-\frac{\varphi_e}{kT}\right), \tag{3.1}$$

where $A = 29$ A (cm^2 K^2)$^{-1}$ with work function $\varphi_e = 2.66$ eV. In the experiment the cathode current density $J_C \approx 13$ A cm^{-2} corresponds to cathode temperature $T_C \sim 1900$ K and is close to the colour temperature of the cathode surface measured with a calibrated colour CCD camera (Sudnikov *et al*. 2017). However, the full cathode current is the sum of electron current from the cathode and of the ion current from plasma. The second one can be estimated from the saturation ion current density measured by a Langmuir probe at $z = 0.4$ m, $j_s(s_{\text{probe}} = 0.6 \cdot \pi \cdot 0.02$ cm$^2) \approx 1.8$ A cm^{-2}. Thus, it is about 13 % of the full cathode current. One needs the secondary electrons to be taken into account ($\gamma_{\text{se}} \approx 0.15$ in LaB_6). As a result, Child's law should be chosen to explain the cathode current behaviour. In this case, one can estimate the gap between the cathode and the virtual plasma anode according to (this distance will be an upper bound of the cathode sheath, and corresponds to the Langmuir sheath):

$$\left.\begin{array}{c} I_{3/2} \approx 1.8 \times 2,33 \cdot 10^{-6}[A/V^{3/2}] \cdot \dfrac{s_C}{d^{*2}} U_{CA^*}^{3/2} \Rightarrow \\ d^* = 0.3 \text{ mm} \end{array}\right\}, \tag{3.2}$$

where $U_{CA^*} = 200$ V, $I_C = 250$ A, the coefficient 1.8 arises for the current in the bipolar diode (see Astrelin & Kotelnikov 2017). If we compare d^* with λ_D (table 1), then the Debye length is significantly less than the calculated sheath layer, as it should be. It should be noted that during the plasma discharge, the cathode surface additional heats up at $\Delta T_C \sim 100$ K owing to ion flux, but it has no influence on the cathode current.

In a situation where the plasma is sufficiently dense and temperature is high, its potential relative to the material wall along the magnetic field should be determined according to the equality of the fluxes of ions and electrons to the wall, i.e. $\Delta\varphi \sim 3.6 \times T_e/e \sim 3.6 \times 40$ eV$/\bar{e} = 140$ V. Based on this, one can draw the axial distribution of 'estimated' potential on the axis of the SMOLA device, see figure 5. The potential growth near the

https://doi.org/10.1017/S0022377821000131 Published online by Cambridge University Press

Parameter		Value	Unit
Debye length	λ_D	15	μm
Electron gyroradius	R_{Le}	1	mm
Ion gyroradius	R_{Li}	40	mm
Electron mean free path relative to gas ionization ($T_e = 40$ eV)	$\lambda_{\mathrm{e\ ion}}$	50	m
1 eV atom mean free path relative to impact ionization ($T_e = 40$ eV)	$\lambda_{\mathrm{H\ ion}}$	8	cm
1 eV atom mean free path relative to charge exchange	$\lambda_{\mathrm{H\ exch}}$	0.2	m
Thermal (500 K) H_2 mean free path relative to impact ionization $H_2 \rightarrow H^+ + H + \bar{e}$	$\lambda_{\mathrm{H_2\ ion}}$	5	mm
Mean free path of electron collision	$\lambda_{\mathrm{e\ tr}}$	3	m
Mean free path of ion collision ($T_i = 4$ eV)	$\lambda_{\mathrm{i\ tr}}$	4	cm
Ion charge-exchange mean free path	$\lambda_{\mathrm{i\ exch}}$	5	m

TABLE 1. Some plasma and particles linear parameters for the described experiment.

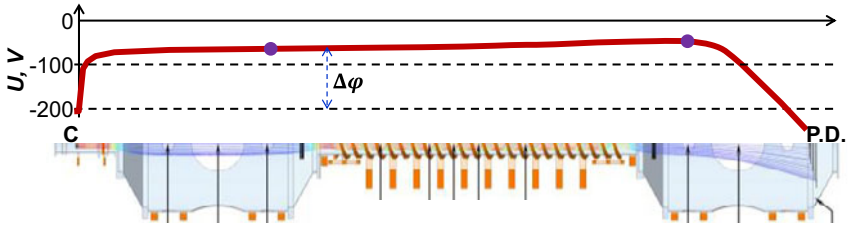

FIGURE 5. Estimation of axial distribution of the plasma potential on the axis. Designations: C, cathode; P.D., plasma dumper. Points: measured data by spectroscopic system. The errors of measurements lie within the points.

cathode occurs at a distance of approximately 0.3 mm. At the exit from the device, owing to the significant magnetic mirror coefficient $R \sim 100$, the plasma flow drops and the plasma cools, which should lead to a smoother growth in potential.

For measurement of the profile of plasma rotation arising owing to the cross-radial electric and confining magnetic field, the spectroscopic diagnostics was created at the facility (Inzhevatkina *et al.* 2019). An example of an H_α emission profile is presented in figure 6. Here one can determine an ion temperature of about 4 ± 0.5 eV, assuming that radiating atoms arise due to the charge exchanging process. At the distance $z = 1.14$ m in our experimental conditions the, diagnostic showed a constant radial angular velocity of

https://doi.org/10.1017/S0022377821000131 Published online by Cambridge University Press

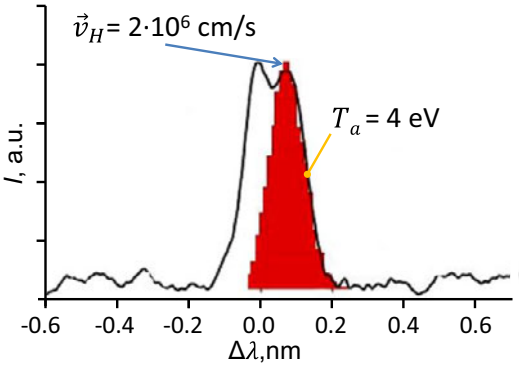

FIGURE 6. The H_α emission profile, measured by a spatial resolving spectroscopic system (Inzhevatkina *et al.* 2019). Red histogram: theoretical Gaussian profile with spectral shift corresponding to the movement of radiating atoms.

plasma rotation with $\omega \approx 8 \times 10^5\ \mathrm{s}^{-1}$. Thus, the rotation speed can be expressed as

$$\omega = \frac{V}{r} = \frac{c}{r}\frac{E}{B} = \text{const.} \tag{3.3}$$

Hence, the potential difference between the axis of the plasma and its periphery is determined by

$$U = \int_0^{r_0} E\,\mathrm{d}r = \int_0^{r_0} \frac{\omega B r}{c}\,\mathrm{d}r = \frac{\omega B}{2c} r_0^2. \tag{3.4}$$

The magnetic field in the diagnostics position is $B = 18.5$ mT, plasma radius is $r_0 \sim 9$ cm:

$$U \approx \frac{8 \cdot 10^5\ \mathrm{s}^{-1} \times 185\ \mathrm{G} \times 81\ \mathrm{cm}^2}{2 \times 3 \cdot 10^{10}\ \mathrm{cm\ s}^{-1}} \approx 60\ \mathrm{V}. \tag{3.5}$$

Summarizing these findings with the assessment of the plasma ambipolar potential, the total voltage drop between the cathode and the electrical grounded device is

$$\Delta U = U + \Delta\varphi = 60\ \mathrm{V} + 140\ \mathrm{V} = 200\ \mathrm{V} \cong U_{\mathrm{CA}}. \tag{3.6}$$

Let us try to describe the distribution of currents in the SMOLA device caused by the plasma source working. As indicated at the beginning of the discussion of the results, the main current in the circuit is of electronic origin. Electrons emitted from the cathode are mainly due to thermionic emission. The cathode current and the cathode sheath are regulated by Child's law according with the virtual plasma anode potential relative to the cathode ($\Delta\varphi \approx 3.6 \cdot T_e/\bar{e} \sim 140$ V). Then, because of the electrons 'trapped' by ambipolar potential on all sides along the magnetic field lines, they oscillate along the system, ionizing the gas and colliding with plasma ions, and drifting outward across the magnetic field. This movement continues until they hit the grounded input plasma limiter.

If we assume that the transverse diffusion of electrons should be provided by electron collision rate and across displacement at the electron gyroradius, then the obtained

https://doi.org/10.1017/S0022377821000131 Published online by Cambridge University Press

transverse current can be estimated as

$$v_{e\perp\text{eff}} = R_{\text{Le}} \times \frac{v_{\text{Te}}}{\lambda_{e\ \text{tr}}} \approx 2 \cdot 10^2 \text{ m s}^{-1}, \tag{3.7}$$

$$I_\perp = v_{e\perp\text{eff}} \cdot n_e \cdot S_\perp \cdot e \approx 200 \text{ A} \sim I_{\text{A}}, \tag{3.8}$$

where $S_\perp \approx 300 \cdot \pi \cdot 0.11$ is the external area of the entire plasma with effective diameter of approximately 11 cm. The measured current flowing on the limiter is about $I_{\text{Lim}} \approx 0.5 \times I_{\text{CA}}$. This confirms that the entire cathode current goes to the limiter according to the kinetics of particle motion across the magnetic field.

It is very interesting to calculate the atoms flux from the gun, considering the fact that by the moment of ignition of the discharge, the density of accumulating H_2 molecules is $n_{H_2} \sim 10^{21}$ m^{-3}. Based on $\lambda_{H_2\ \text{ion}} \approx 5$ mm, table 1, it follows that the H_2 molecules immediately getting into the plasma near the cathode dissociates into fast atoms and the one of them is ionized. In this case, only half of the molecules make it possible to form a flow of fast atoms, with the remaining flux as ions. Therefore, a source of fast approximately 1 eV atoms with the density $n_a \approx 10^{21}$ m^{-3}, the mean free path of which relative to ionization $\lambda_{\text{H ion}} = 8$ cm, table 1, must be placed in the cathode region. As $\lambda_{\text{H ion}}$ only varies by a factor of 2.5 from the length of the gun's transport channel and also taking the gun's channel diameter as 6 cm, the hydrogen atoms flux can be estimated as

$$\begin{aligned} J_G &\approx J_0 \cdot \Delta\Omega_n \cdot exp(-2.5) = 10^6 \sqrt{T_a} n_a \delta s \times \Delta\Omega_n \cdot exp(-2.5) \\ &= 0.8 \cdot 10^{19} \text{ atoms s}^{-1} = 1.3 \text{ eq.A}, \end{aligned} \tag{3.9}$$

where $\Delta\Omega_n = \pi \cdot 3^2/2\pi \cdot 20^2$ corresponds to a spherically symmetric expansion of particles and the cutting of this flow by the anode diaphragm, $\delta s \approx 9$ cm^2, which is the cross-section of the gap between the cathode and the nearest diaphragm. Comparing with the gun fed by the working gas during the operation of a 'slow' valve $J_{\text{feed}} \approx 20$ eq.A, it is less than 10%. This means that gas supply is spent mainly on the plasma flux creation in the SMOLA device.

The stationary gas puffing must be in agreement with the vacuum pressures in the expanders and its pumping rates, i.e. $J_{\text{feed}} \approx 20$ eq.A $\approx n_1 U_p + n_2 U_p$, where $n_{1,2}$ is the gas density in the expanders (entrance and exit) and $U_p = 2$ m^3 s^{-1} is the regular pumping speed. The gas pressure measurements of approximately 6 and 4 mPa (see figure 3, curves 9 and 10) in the entrance and exit expanders, correspondingly, give the gas densities of $n_{1,2} \approx \{1.5; 1\} \times 10^{18}$ m^{-3}. As result, $n_1 U_p + n_2 U_p \approx 1.6$ eq.A, which is quite small in comparison with the gun feeding $J_{\text{feed}} \approx 20$ eq.A. These inconsistent values could be explained by the surface pumping action of plasma dumpers, when exposed by fast ions, of about several tens of electronvolts, from the plasma. The fast ions can arise when there is sufficient electric field near the surface, which is in accordance with the estimation of axial distribution of the plasma potential in figure 5.

So far, we have discussed the quasi-stationary discharge region within 70 ms $< t <$ 213 ms. However, in the period of $0 < t < 70$ ms, a transient process occurs, which is also interesting from the point of view of the discharge creation and gas conditions in the system. Thus, on the pressure signal in the exit expander there is an increase in the gas leakage rate in the period $t_1 \approx 30$ ms to $t_2 \approx 40$ ms from the moment of the discharge ignition. This is associated with the effect of the gas flow increasing from the plasma gun, which should increase the effective temperature of the gas. In this case, the amount of pulsed puffing gas can be estimated. The difference in gas leakage rates before and after time t_1, as well as time $\Delta t = t_1 - t_2 \approx 10$ ms, gives an additional increase

https://doi.org/10.1017/S0022377821000131 Published online by Cambridge University Press

in gas molecules $\Delta N_{H_2} \approx 2.3 \times 10^{18}$. It corresponds to a gas density in the plasma gun of $n^*_{H_2} \sim \Delta N_{H_2}/V_G \sim 0.5 \cdot 10^{21}$ m^{-3}, and it is about half the amount of gas in the gun before discharge ignition. After plasma termination at 213 ms $< t <$ 260 ms, the pressure in the entrance expander rises quickly. The amount of injected gas giving this rise corresponds to the gas portion remaining in the gun volume before this moment. The absence of increasing pressure in the exit expander confirms this assumption, because there is a long vacuum tube between the expanders, which inhibits gas pressure from rising quickly.

The rise in gas pressure during $t_1 < t < t_2$ is immediately compensated for by the appearance of the plasma and the beginning of its operation as a vacuum pump. The gas entering it must be effectively ionized, and, as was written previously, block the direct gas flux from the gun into the entrance expander.

The calculated gas flow from the plasma gun during the stationary state of operation $J_G \approx 0.8 \times 10^{19}$ atoms s^{-1} should be in accordance with the pressure of approximately 3 mPa ($n^{(exp)}_{H_2} = 7 \times 10^{17}$ m^{-3}, eq.) in the entrance expander through the pumping speed, i.e. $J \approx n_{H_2} \cdot U$. As result, we can estimate the rate of gas pumping in the system $U \approx J_G/n_{H_2} \approx 11$ m^3 s^{-1}. This speed significantly exceeds the pumping speed of the installed regular pump $U_p = 2$ m^3 s^{-1}. However, the presence of plasma in the system can itself can 'work' as a vacuum pump. In our case, the plasma pumping rate, based on the small mean free path of hydrogen molecules through the plasma, can be estimated as $U \approx 600$ m s^{-1} $\cdot$ $S_{eff} \approx 60$ m^3 s^{-1}, where $S_{eff} \sim 0.5 \times 0.2$ m^2 is the effective plasma surface in the input expander. Owing to this value, one can explain the resulting gas pressure in the system.

4. Conclusion

As a result of the work, it can be objectively stated that the developed plasma source successfully deals with the task of plasma creation in the SMOLA device. The duration of plasma generation of 1.5 s is limited only by the electric power supply system. The plasma density in the device reaches up to $n_i \approx 10^{19}$ m^{-3} on the axis of the system and it is somewhat non-isothermal between the components $T_e \sim 40$ eV, $T_i \sim 4$ eV. However, it does not affect the process of plasma transport in the helicoidal system.

Data availability statement

The data that supports the findings of this study are available within the article, but the supplementary data that seem appropriate to the reader are available from the corresponding author upon reasonable request.

Acknowledgements

The upgrade of power supply systems for the increase of the discharge duration up to 1 s was supported by the Ministry of Science and Higher Education of the Russian Federation.

All authors contributed equally to analysing data and reaching conclusions, and in writing the paper.

Editor William Dorland thanks the referees for their advice in evaluating this article.

Declaration of interests

The authors report no conflict of interest.

Funding

This work was supported by the Russian Science Foundation (project No. 18-72-10080).

REFERENCES

Akhmetov, T. D., Davydenko, V. I., Ivanov, A. A., Kreter, A., Mishagin, V. V., Savkin, V. Y., Shulzhenko, G. I. & Unterberg, B. 2016 Arc discharge plasma source with plane segmented LaB6 cathode. *Rev. Sci. Instrum*. **87**, 056106.

Anikeev, A. V., *et al.* 2015 Progress in mirror-based fusion neutron source development. *Materials* **8**, 8452–8459.

Astrelin, V. T. & Kotelnikov, I. A. 2017 Boundary conditions on the plasma emitter surface in the presence of a particle counter flow: I. Ion emitter. *Plasma Phys. Rep*. **43**, 129–140.

Bagryansky, P. A., *et al.* 2015 Overview of ECR plasma heating experiment in the GDT magnetic mirror. *Nucl. Fusion* **55**, 053009.

Beklemishev, A. D. 2013 Helicoidal system for axial plasma pumping in linear traps. *Fusion Sci. Technol*. **63** (1T), 355–357.

Beklemishev, A. D. 2015 Helical plasma thruster. *Phys. Plasmas* **22**, 103506.

Beklemishev, A. D. 2016 Radial and axial transport in trap sections with helical corrugation. *AIP Conf. Proc*. **1771** (2016), 040006.

Binderbauer, M. W., *et al.* 2015 A high performance field-reversed configuration. *Phys. Plasmas* **22**, 056110.

Conyers Herring & Nichols, M. H. 1949 Thermionic emission. *Rev. Mod. Phys*. **21**, 185–270.

Gekelman, W., *et al.* 2016 The upgraded large plasma device, a machine for studying frontier basic plasma physics. *Rev. Sci. Instrum*. **87**, 025105.

Goebel, D. M., Hirooka, Y. & Sketchley, T. A. 1985 Large area lanthanum hexaboride electron emitter. *Rev. Sci. Instrum*. **56**, 1717.

Gota, H., *et al.* 2019 Formation of hot, stable, long-lived field-reversed configuration plasmas on the C-2W device. *Nucl. Fusion* **59** (11).

Inzhevatkina, A. A., Burdakov, A. V., Ivanov, I. A., Postupaev, V. V. & Sudnikov, A. V. 2019 Doppler spectroscopy system for the plasma velocity measurements in SMOLA helical mirror. *Plasma Fusion Res*. **14**, 2402020.

Kreter, A., Brandt, C., Huber, A., Kraus, S., Möller, S., Reinhart, M., Schweer, B., Sergienko, G. & Unterberg, B. 2017 Linear plasma device PSI-2 for plasma-material interaction studies. *Fusion Sci. Technol*. **68**, 8–14.

Lafferty, J. M. 1951 Boride cathodes. *J. Appl. Phys*. **22**, 299.

Postupaev, V. V., Batkin, V. I., Beklemishev, A. D., Burdakov, A. V., Burmasov, V. S., Chernoshtanov, I. S., Gorbovsky, A. I., Ivanov, I. A., Kuklin, K. N. & Mekler, K. I. 2017 The GOL-NB program: further steps in multiple-mirror confinement research. *Nucl. Fusion* **57**, 036012.

Postupaev, V. V., Sudnikov, A. V., Beklemishev, A. D. & Ivanov, I. A. 2016 Helical mirrors for active plasma flow suppression in linear magnetic traps. *Fusion Engng Des*. **106**, 29–33.

Simonen, T. C., Anikeev, A., Bagryansky, P., Beklemishev, A., Ivanov, A., Lizunov, A., Maximov, V., Prikhodko, V. & Tsidulko, Y. 2010 High beta experiments in the GDT axisymmetric magnetic mirror. *J. Fusion Energy* **29**, 558–560.

Sudnikov, A. V., Beklemishev, A. D., Postupaev, V. V., Burdakov, A. V., Ivanov, I. A., Vasilyeva, N. G., Kuklin, K. N. & Sidorov, E. N. 2017*a* SMOLA device for helical mirror concept exploration. *Fusion Engng Des*. **122**, 86–93.

Sudnikov, A. V., Beklemishev, A. D., Postupaev, V. V., Ivanov, I. A., Burdakov, A. V., Inzhevatkina, A. A. & Zhuravlev, N. A. 2017*b* Status and program of concept exploration helical mirror device. In *Proceedings of the 44th EPS Conference on Plasma Physics*, P1.139. Available at: http://ocs.ciemat.es/EPS2017PAP/pdf/P1.139.pdf

Sudnikov, A. V., Beklemishev, A. D., Postupaev, V. V., Ivanov, I. A., Inzhevatkina, A. A., Sklyarov, V. F., Burdakov, A. V., Kuklin, K. N., Rovenskikh, A. F. & Melnikov, N. A. 2019 First experimental campaign on SMOLA helical mirror. *Plasma Fusion Res*. **14**, 2402023.